TU Delft

Delft University of Technology

Corrosion-fatigue damage identification in submerged mooring chain links using remote acoustic emission monitoring

Riccioli, Filippo; Gabrielsen, Øystein; Høgsæt, Ingrid Skutle; Barros, Pedro Silva; Pahlavan, Lotfollah

DOI
10.1016/j.marstruc.2024.103685

Publication date
2024

Document Version
Final published version

Published in
Marine Structures

Citation (APA)
Riccioli, F., Gabrielsen, Ø., Høgsæt, I. S., Barros, P. S., & Pahlavan, L. (2024). Corrosion-fatigue damage identification in submerged mooring chain links using remote acoustic emission monitoring. *Marine Structures*, *98*, Article 103685. https://doi.org/10.1016/j.marstruc.2024.103685

Important note
To cite this publication, please use the final published version (if applicable).
Please check the document version above.

Copyright
Other than for strictly personal use, it is not permitted to download, forward or distribute the text or part of it, without the consent of the author(s) and/or copyright holder(s), unless the work is under an open content license such as Creative Commons.

Takedown policy
Please contact us and provide details if you believe this document breaches copyrights.
We will remove access to the work immediately and investigate your claim.

This work is downloaded from Delft University of Technology.
For technical reasons the number of authors shown on this cover page is limited to a maximum of 10.

Marine Structures 98 (2024) 103685

Contents lists available at ScienceDirect

Marine Structures

journal homepage: www.elsevier.com/locate/marstruc

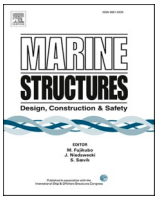

Corrosion-fatigue damage identification in submerged mooring chain links using remote acoustic emission monitoring

Filippo Riccioli [a,*], Øystein Gabrielsen [b], Ingrid Skutle Høgsæt [c], Pedro Silva Barros [c], Lotfollah Pahlavan [a]

[a] Department of Maritime and Transport Technology, Delft University of Technology, 2628CD, Delft, the Netherlands
[b] Equinor ASA, Arkitekt Ebbells veg 10, 7053, Ranheim, Norway
[c] DNV (Det Norske Veritas), Veritasveien 1, 1363, Høvik, Norway

ARTICLE INFO

Keywords:
Acoustic emission
Corrosion-fatigue
Damage localisation
Mooring chain
Structural health monitoring

ABSTRACT

This paper investigates the feasibility of detection, localisation, and monitoring of corrosion-fatigue damage in mooring chain links using remote Acoustic Emission (AE) technique in submerged conditions. A large-scale experiment was conducted on a studless R4 chain retrieved after about two decades of operation offshore. Ultrasound signals were continuously measured using fixed and movable arrays of AE transducers placed on perpendicular planes in the water tank enclosing the chain. The AE parameters extracted from the measured signals have been analysed. AE sources were successfully localised on the 3D geometry of the chain links. The results suggest that damage growth can be detected and localised using non-contact underwater AE transducers.

1. Introduction

Mooring chains are key assets for offshore floating energy production systems, e.g. wind turbines, photovoltaic islands, and floating production-storage-offloading units (FPSOs). Corrosion, fatigue, and corrosion-enhanced fatigue, i.e. corrosion-fatigue, are regarded as the predominant degradation mechanisms affecting the structural integrity of mooring chains [1–6]. Fig. 1 shows examples of fatigue cracks and corrosion pits on the surface of a chain link. Structural integrity assessment of mooring chains can be challenging due to their difficult access and the required arrangements for subsea inspections. Furthermore, due to the presence of marine growth on the surface of the chain links, often surface cleaning is necessary to perform a detailed assessment. This process is generally undesirable from technical, economic, and environmental points of view.

A number of methods have so far been proposed for non-intrusive integrity assessment of mooring chains, however with suboptimum reliability in the detection of corrosion-fatigue damage. For example, visual inspection can be performed after cleaning the surface [7]. However, only relatively large-sized surface defects (in the order of mm) can be detected by this technique. The results of the inspection can also be affected by the clarity of the seawater, and it often needs further damage inspection using more advanced NDT methods after surface cleaning. Magnetic Particle Inspection (MPI) may be used to detect surface and near-surface flaws in ferromagnetic materials [8–11]. Results of the analysis, such as the true length of discontinuities, may be obtained with reasonable accuracy [12]. Nonetheless, deeply embedded flaws cannot be detected using this technique, and application of the method also requires surface cleaning [7]. Magnetic Flux Leakage (MFL) can identify defects deeper within the material, but only where the clean

* Corresponding author. Delft University of Technology, Mekelweg 2, 2628CD, Delft, the Netherlands.
E-mail address: f.riccioli@tudelft.nl (F. Riccioli).

https://doi.org/10.1016/j.marstruc.2024.103685
Received 12 May 2024; Received in revised form 8 August 2024; Accepted 26 August 2024
Available online 31 August 2024
0951-8339/© 2024 The Authors. Published by Elsevier Ltd. This is an open access article under the CC BY license (http://creativecommons.org/licenses/by/4.0/).

material surface can be accessed. Ultrasonic testing can also detect and size surface and subsurface defects and can be employed for inspection of welds [8,9]. Guided ultrasonic waves (GUWs) offer possibilities to locate cracks and notches probing larger areas of the structure from a few monitoring points. This method requires proper coupling between the material surface (after preparation, i.e. cleaning) and probes. Generally, the accuracy and reliability of all the above-mentioned methods are adversely affected by the presence of corrosion pits on the surface (Fig. 1). Note that radiography techniques can also detect internal and surface defects by imaging the internal structure of the assessed material using high-energy electromagnetic waves [12]. Nevertheless, subsea utilisation of this technique is very limited due to safety hazards and environmental concerns [8].

Acoustic Emission (AE), a passive ultrasound method, is an established technique to detect and monitor corrosion, fatigue, and corrosion-fatigue using surface-bonded transducers [13–18]. AE can enable the identification, localisation, and characterisation of damage by continuously monitoring the transient stress waves generated by the rapid release of energy from localised sources within the material [19]. High-frequency elastic waves are often captured by piezoelectric sensors, typically in contact with the material surface. Measuring the arrival time of the waves at different sensors enables the localisation of AE sources in the material. Every localised AE event can be related to the onset of new damage or the progression of an active fault in the material structure. Several authors performed small-scale experiments to characterise the corrosion- and corrosion-fatigue-induced AE sources [13,20–36]. Despite the promising results in corrosion-fatigue damage detection and monitoring using AE, only a few large-scale testing attempts have been made using mooring chains. Rivera et al. [37] conducted a long-term (4-month) chain tensile test to assess the feasibility of monitoring crack initiation and growth in mooring chain links in artificial seawater using the AE technique. The authors identified the cumulative hits (i.e. cumulative number of AE signals measured throughout the test [13]) as one of the most promising AE parameters for continuous monitoring of damage initiation and propagation in mooring chain links. Angulo et al. [38] performed a 72-day large-scale fatigue experiment to assess the capabilities of AE as a monitoring tool to detect crack initiation and propagation in mooring chains under realistic loading and environmental conditions. The authors pointed out the frequency content of the ultrasound signals as the most promising parameter to detect growing damage in the chain links. An increase in the average frequency (i.e. ratio between signal counts and duration [13]) was observed with the growth of the crack in the chain link. However, the difficult environment and the high level of noise recorded during the experiment represented a challenge for a full and comprehensive analysis of the measurements. Limited investigations on the detection and monitoring of ultrasound signals using non-contact AE technique have also been reported in the literature, see for example [39–42]. Recently, the authors have investigated the detectability of AE signals during accelerated corrosion and corrosion-fatigue processes using non-contact AE transducers on small-scale specimens underwater [43,44].

This paper presents a feasibility study of detecting, localising, and monitoring corrosion-fatigue damage in full-scale mooring chain links using underwater non-contact AE measurements. Large-scale corrosion-fatigue experiments have been conducted on a 5-link mooring chain segment. Ultrasound signals have been measured using a fixed vertical array of AE transducers and two movable groups of AE transducers facing the chain from two perpendicular planes. The AE parameters extracted from the measured signals have been analysed throughout the duration of the test. A 3D source localisation algorithm for the corrosion-fatigue-induced ultrasound signals has been implemented. The detected damage zones agree with the post-failure observation in the mooring chain links.

The paper has the following structure. An overview of AE monitoring and source localisation is presented in Section 2. A description of the experiments is given in Section 3. Results are presented and discussed in Section 4, followed by conclusions in Section 5.

2. Methodology

The methodology of AE monitoring in this investigation comprises parametrisation of AE signals as well as localisation of AE sources as described below.

2.1. AE monitoring of corrosion-fatigue damage

Parametrisation of the AE signals [13,26] is used in this study to monitor the acoustic activity induced by initiation and growth of corrosion-fatigue damage. Damage-induced ultrasound signals have been continuously recorded using a vertical array of four AE

Fig. 1. Fatigue crack (left) and corrosion pits (right) in mooring chain links.

transducers (deployed over the length of the chain segment) throughout the test. The analysis covers 100 h of measurements sampled uniformly throughout the test. The total number of AE signals, the cumulative number of AE signals, and the AE hit rate (defined as the number of burst-type signals [45,46] per loading cycle) have been analysed over the test duration. The total number of AE signals provides insights into the most active areas along the chain segment. The analysis of the cumulative number of AE signals over the test duration enables the assessment of the evolution of the damage-induced signals throughout the test. A relatively steep curve of the cumulative number of signals may be expected during crack initiation and stable growth. Besides that, the AE hit rate is employed to identify active damage zones. Every AE event can indicate the onset of new damage or the progression of an existing active defect in the material. The variation of the AE hit rate during the test provides insights into the damage growth rate.

2.2. AE source localisation

The AE source localisation approach in this study utilises the principle of triangulation [47]. In this process, for every AE event, the differential time-of-flight at each sensor is obtained from the waveforms using the Akaike Information Criterion (AIC) [48,49]. Minimising the error between the predicted and measured differential arrival times over the domain is performed to estimate the source location.

For an arbitrary point with coordinates $\mathbf{x}$ belonging to the domain Ω defined by the surface of the chain links, the error function, i.e. objective function, is defined as follows:

$$e_k(\mathbf{x}) = \left(\sum_{i=1}^{M_k} \left\| \frac{1}{c_w} (\|\mathbf{x} - \mathbf{x}_i\| - \|\mathbf{x} - \mathbf{x}_r\|) - \tau_i \right\|^2 \right)^{\frac{1}{2}}, \tag{1}$$

where M_k is the number of sensors participating in the localisation of the *kth* AE event, $\mathbf{x}_i$ is the vector containing their coordinates and $\mathbf{x}_r$ indicates the coordinates of the (arbitrarily chosen) reference sensor r. c_w denotes the speed of sound in water. τ_i expresses the differential arrival time of the ultrasound signals at sensor i (participating in the recording of the AE event) with respect to the reference sensor.

The most probable location of the source signal $\mathbf{x}_k^s$ can therefore be obtained as:

$$\mathbf{x}_k^s = \text{argmin} e_k(\mathbf{x}) \quad \mathbf{x} \in \Omega. \tag{2}$$

A maximum allowable error value can be additionally used as a quality criterion to improve the reliability of the source localisation. For the coupled movable arrays of AE transducers holding eight transducers on perpendicular planes (shown in Fig. 2),

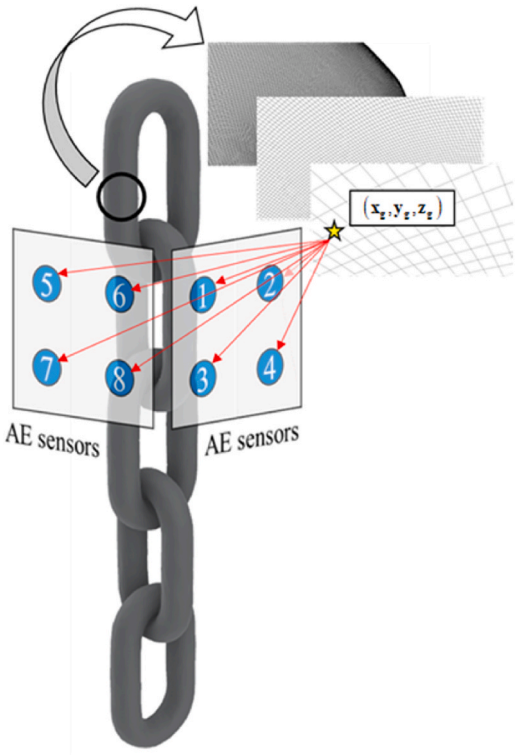

Fig. 2. Schematic illustration of the sensor holders and the localisation approach. The sensor holders are coupled and move simultaneously.

participation of a minimum of 3 sensors was considered. Once the procedure described above is applied to all AE events, a cumulative normalised inverse error function (ε) is defined for the visualisation of the most probable location of the AE source over the entire measurement period:

$$\varepsilon = \sum_{k=1}^{N} \alpha_k \beta_k e_k^{-1}(\boldsymbol{x}), \tag{3}$$

$$\beta_k = \begin{cases} 0, & \forall e_k > \bar{e}_k \\ 1, & \forall e_k \leq \bar{e}_k \end{cases}, \tag{4}$$

where N is the total number of localised AE events, and α_k is the normalisation factor limiting the values of $e_k^{-1}(\boldsymbol{x})$ to [0,1], and β_k is a binary coefficient that selects only the events that satisfy the localisation error threshold.

The scheme described above has been numerically implemented by discretizing the domain Ω. A 3D model of the chain surface obtained with 3D laser scanning has been used for this purpose.

3. Materials and methods

A 5-link mooring chain segment was subjected to cyclic loading while submerged in artificial seawater to detect and localise damage-induced ultrasound signals using remote AE measurements.

3.1. Experimental set-up and test specimen

A vertical test rig was used to perform fatigue testing of a 5-link mooring chain retrieved after operation offshore. The chain sample consists of a segment of a studless R4 chain with a nominal diameter of 137 mm and a nominal Minimum Breaking Load (MBL) of 16992 kN. The chain segment was submerged in artificial seawater, i.e. a 3.5 ± 0.1 wt-% sodium chloride aqueous solution, while subjected to cyclic loading. The fatigue test was run in load control. The key parameters for the fatigue experiment are summarised in Table 1. The vertical test rig was instrumented with non-contact watertight AE transducers to continuously measure damage-induced ultrasound signals during the experiment (Fig. 3).

3.2. AE testing

A vertical array of AE transducers was deployed along the length of the chain sample (Fig. 3). The vertical array was placed at a fixed distance from the chain sample and held in position by a combination of sensor holders and carabiners. Two movable arrays of AE transducers were deployed on two perpendicular planes on the front and left sides of the chain sample (Fig. 4). The movable arrays of transducers consist of two groups of AE sensors (each at a fixed distance from the chain) with a controllable vertical position. The movable arrays were connected to a separate mechanism to make stops in front of different chain links. Each movable array was held in position using a sensor holder and two polyester lines (on the sides of the sensor holder) to constrain its rotation around the vertical axis. A centre line (orange rope in Figs. 3 and 4) was used to control the vertical position of each sensor holder.

An AMSY-6 Vallen data acquisition (DAQ) system was used to collect and record the damage-induced signals during the experiment. Twelve watertight piezoelectric AE transducers (VS150-WIC-V01, with an integrated preamplifier, gain of 34 dB) were connected to the DAQs using watertight co-axial cables. The AE sensors were resonant piezoelectric transducers with resonant frequency of 150 kHz and an operating frequency range of 50–450 kHz [37,38,43]. The transfer function of the transducers can be found in Alkhateeb et al. [43]. The signals were recorded using a sampling rate of 2.5 MHz (with a total sample length of 4096 points). AE signals were continuously measured throughout the entire experiment. The results presented in the study refer to 100 h of AE measurements sampled equally over the test duration. Fig. 5 shows a schematic illustration of the sensors layout and the positions of the movable arrays of transducers during the experiment.

The movements of the two arrays were synchronised and performed manually every 24 h during the experiment. Seven positions were defined before testing (Fig. 5). The positions correspond to the 4 link-to-link areas (typically the most susceptible zones to damage in mooring chain links) and 3 flash butt weld regions. The time spent in each position is given in Table 2 as a percentage of the total hours of measurements analysed.

Before the start of the test pencil lead break tests were performed (according to ASTM E976-15 [50]) at different locations on the

Table 1
Test parameters.

Chain diameter [mm]	137
Chain grade	R4
MBL [kN]	16992
Environment	Artificial seawater (3.5 % NaCl)
Middle load [%MBL]	9.4
Load amplitude [%MBL]	4.8
Test frequency [Hz]	0.5

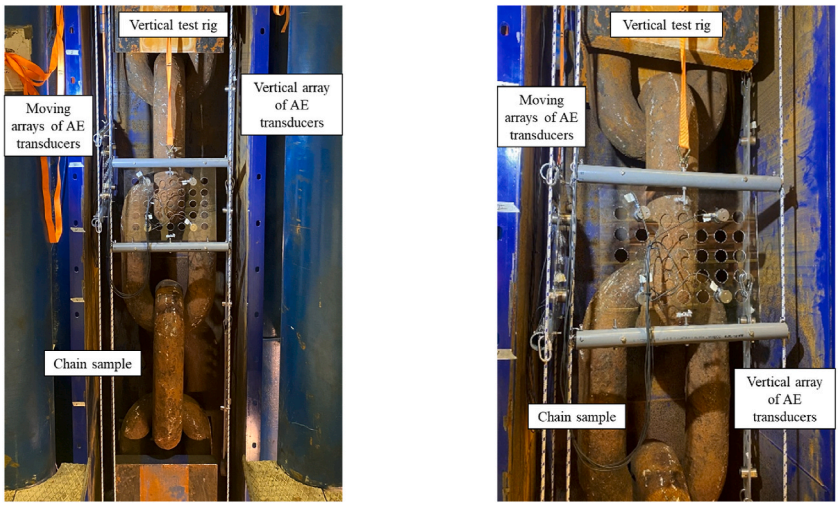

Fig. 3. Instrumented test rig (left) and non-contact sensors deployment in the test rig (right).

Fig. 4. Perpendicular movable arrays of AE transducers.

external side of the closed tank (after filling with artificial seawater) to verify the reproducibility of the AE sensors response in water and proper operation of the AE measurements system.

During the commissioning process, the noise level was assessed. Cyclic loads (using the same loading conditions shown in Table 1) were applied to the chain sample submerged in artificial seawater. The measured noise level was about 50 dB. The acquisition threshold was hence set to 60 dB.

The recorded ultrasound signals were pre-processed using a signal-to-noise ratio (SNR) filter of 20 dB to separate potential damage signals from background noise (i.e. continuous-type signals [45,46]).

4. Results and discussion

Experiments described in Section 3 were performed and the methodology for the analysis of the ultrasound signals described in Section 2 was applied. The present analysis includes ultrasound signals recorded during 100 h of testing. To ensure even distribution, the measurement hours were chosen to span the entire duration of the experiment.

4.1. Detection and monitoring of corrosion-fatigue damage

Parametrisation of the AE measurements provides general insights into the acoustic activity recorded in the test rig throughout the test. The vertical array of four AE transducers is used to detect and monitor possible damage zones along the chain segment.

Fig. 6 shows the total number of AE signals (Fig. 6a) and the cumulative number of AE signals recorded by the vertical array of

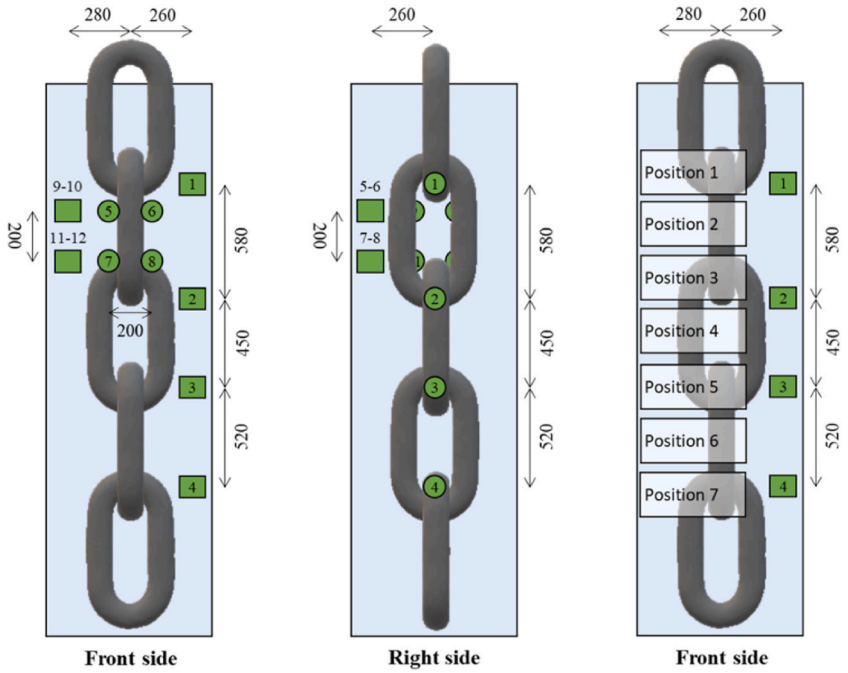

Fig. 5. Schematic illustration of the AE sensors layout and positions of movable arrays. Dimensions in mm.

Table 2
Measurement time spent in each position by the movable arrays of transducers and used to calculate the localisation map of AE sources. The time is expressed as a percentage of the total hours of measurements analysed.

Position 1	25 %
Position 2	11 %
Position 3	22 %
Position 4	11 %
Position 5	18 %
Position 6	7 %
Position 7	6 %

transducers (Fig. 6b) along with the normalised vertical displacement throughout the test.

The total number of AE signals indicates sensor 1 as the most active in the vertical array pointing out Link 1–2 as the most active area in the test rig. This can be due to the combination of main damage-induced ultrasound signals with noise signals from the upper clamp of the test rig. On the other hand, the latter is expected to be limited by the SNR-based filter used in the pre-processing of the data. The acoustic activity decays toward the bottom of the test rig. However, sensor 4 shows increased activity compared to sensor 3 possibly due to noise generated by the clamp and the water inlet at the bottom of the test rig.

The cumulative number of AE signals shows a clear distinction between the activity in the top part of the chain segment and the mid-lower one. The slope of the cumulative trend is represented by the AE hit rate (in Fig. 7). Note that in previous research, the correlation between crack growth and AE hit rate has been demonstrated [51,52] and the slope of cumulative AE parameters has been used to identify different crack growth stages [21,26]. Sensor 1 displays a relatively steep curve throughout the experiment. In particular, two slopes can be observed. First from 0 % to 35 %, and second from 45 % to 85 % of the test duration. This could indicate a corrosion-fatigue damage growth at two different rates between 0-35 % and 45–85 %, respectively. During the latest stage of the test, a characteristic AE quiescence is observed. Besides that, sensors 2–4 show relatively similar trends that differ from the one followed by sensor 1. The cumulative number of signals measured by sensors 2–4 undergoes a steep increase between 0 and 15 % of the test duration while it has a very low slope during the remaining part of the experiment. The AE activity at the initial part of the test could be related to crack formation. There seems to be a correlation between the local jumps in the elongation curve and changes in the slope of the cumulative number of AE signals in different channels. A more detailed assessment of the correlation however would require the selection of the AE events per damage location, hence not discussed further in this section.

Fig. 7 shows the AE hit rate for the vertical array of transducers. Sensor 1 displays an AE hit rate value of 0.7–0.8 signals per cycle from 0 % to about 35 % of test duration. The AE hit rate jumps above 1 signal per cycle after 35 % of the test duration. This possibly

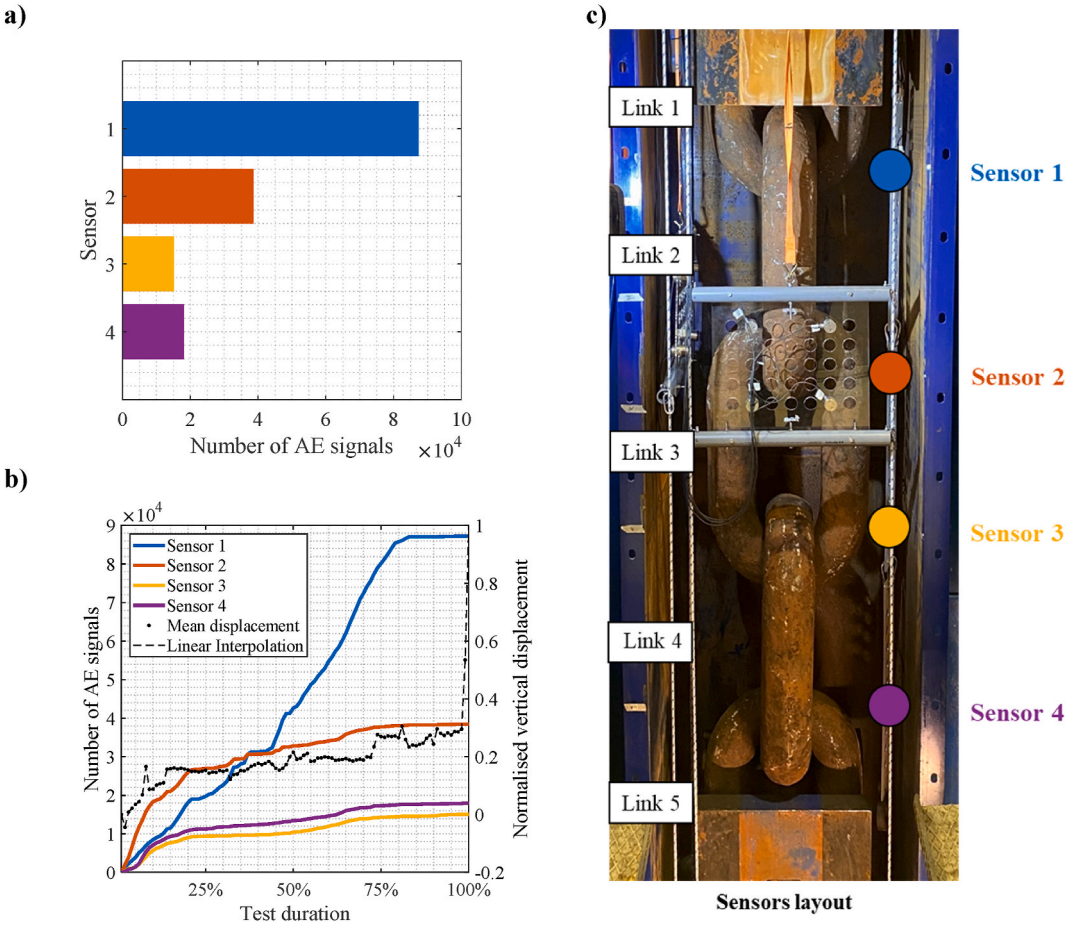

Fig. 6. (a) Total number of AE signals and (b) cumulative number of AE signals measured by the vertical arrays of transducers and normalised vertical displacement throughout the test. (c) Layout of the vertical array of transducers.

indicates two different rates of crack growth. After 85 % of the experiment, the hit rate level drastically decreases (i.e. AE quiescence). Sensors 2–4 show relatively similar behaviour between each other. Initially, they present an AE hit rate level in the range (that is the case for sensors 3 and 4) or even higher (see sensor 2) than the one of sensor 1. After about 25 % of the test duration, however, the hit rate does not exceed 0.5 signal per cycle (suggesting an average of 1 hit per every two load cycles).

4.2. Damage localisation

Damage-induced ultrasound signals have been localised using two movable arrays of AE transducers deployed on perpendicular planes. Results of the AE source localisation were projected on the 3D geometry of the chain segment in the form of a localisation map. The AE source localisation map has been calculated using the procedure described in Section 2, and calculated over the grid points for each localised event for all the positions of the movable arrays. The grid has a uniform spacing of 10 mm in x, y, and z directions. The speed of sound in water is considered to be 1500 m/s at 20 °C. Also, a maximum allowable error (between the predicted and the actual differential arrival times of the wave) of 10 μs has been used.

Fig. 8 shows the localisation map for four time periods of the test duration. Only from the AE source localisation maps, three damage zones can be identified. The damage zones are defined as the areas in the chain segment showing the highest number of localised AE events. These zones are located at the intersections of neighbouring links (i.e. Link 1–2, Link 2–3, and Link 3–4) and can generally be interpreted as the 'crown areas' (generally being the most susceptible to cracks, along with the welds). The first part of the test, 0–25 % of test duration, shows localised acoustic activity between Link 1–2 and Link 2–3. Both zones present a range of 250–300 localised AE events. In the second part of the test, 25–50 % of the test duration, the largest area of AE activity is located between Link 3–4, with 120–150 AE events. Between 50 and 75 % of the test duration, a relatively high number of AE events (in the order of 300–400) is localised around the crown area of Link 2, towards Link 1. The final part of the experiment, between 75 and 100 % of the test duration, shows acoustic activity in the upper crown of Link 4, with 50–80 AE events.

Fig. 9 shows the localisation map for the 100 h of measurements analysed. The AE source localisation map reveals three distinct zones of acoustic activity. Acoustic activity is expected to have been detected all over the chain segment due to the natural corrosion

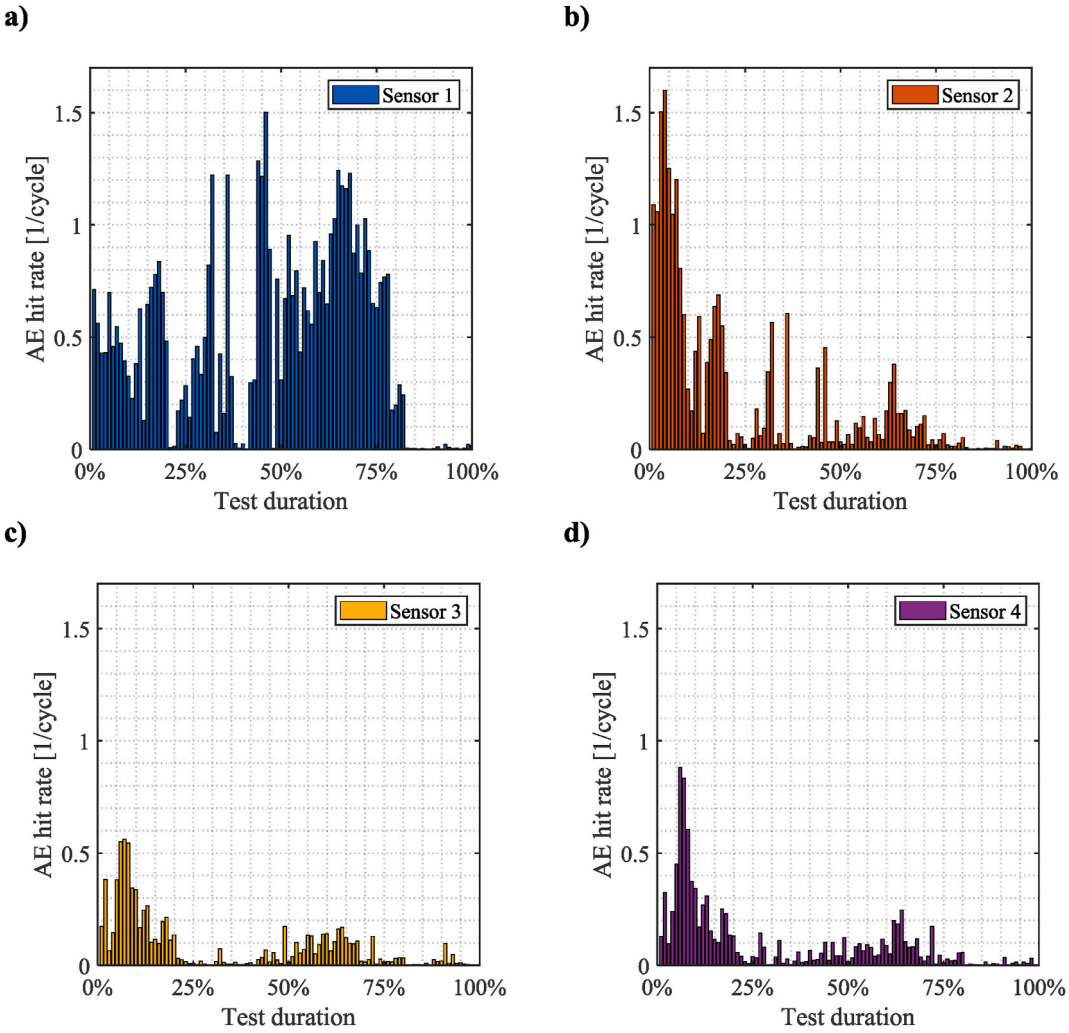

Fig. 7. AE hit rate measured by the vertical array of AE transducers.

process. However, highly localised AE activity can manifest the presence of fatigue cracks. The most prominent localised area is observed in Link 1–2. This is characterised by a number of localised AE events of approximately 600, spread between the crown and the weld area of Link 2. The second-largest area of AE activity is situated in the crown area of Link 2, towards Link 3, with 550–600 localised AE events. These initial observations suggest that Link 1–3 was the most acoustically active part of the chain, confirming early indications from the parametric analysis of AE. A third zone of activity is noted in the crown of Link 4, toward Link 3, accounting for a total of localised AE events ranging between 450 and 500. A few limitations and improvement points can be identified in the AE source localisation map. First, the localised areas seem to be biased against the middle part of the chain link crown (where fatigue crack is expected to grow). This bias may arise from potential masking effects on the damage-induced ultrasound signals and the limited number of sensors in play in the localisation. Possible improvements involve increasing the number of sensors in the movable arrays and accounting for masking issues in the AE source localisation algorithm. Second, the difference in AE events numbers may be related to the extent and stage of damage, but it is also influenced by the sensitivity of the sensors and the monitoring duration in each specific position (of the movable array). Future work will incorporate the normalisation of the AE source localisation map to enhance a more accurate comparison of the monitoring results.

4.3. Post-failure inspection

The condition of the chain segment was assessed at the end of the experiment through visual inspection and magnetic particle (MP) testing. All the links of the chain segment were tested. The positions in each link are labelled A, B, C, and D as shown in Fig. 10. The reported observations are located in the crown area of the chain links. The results of the post-failure inspection are shown in Fig. 11. The main fracture (Fig. 11a) was observed in Link 1 towards Link 2. The results of the post-failure inspection are summarised in Table 3.

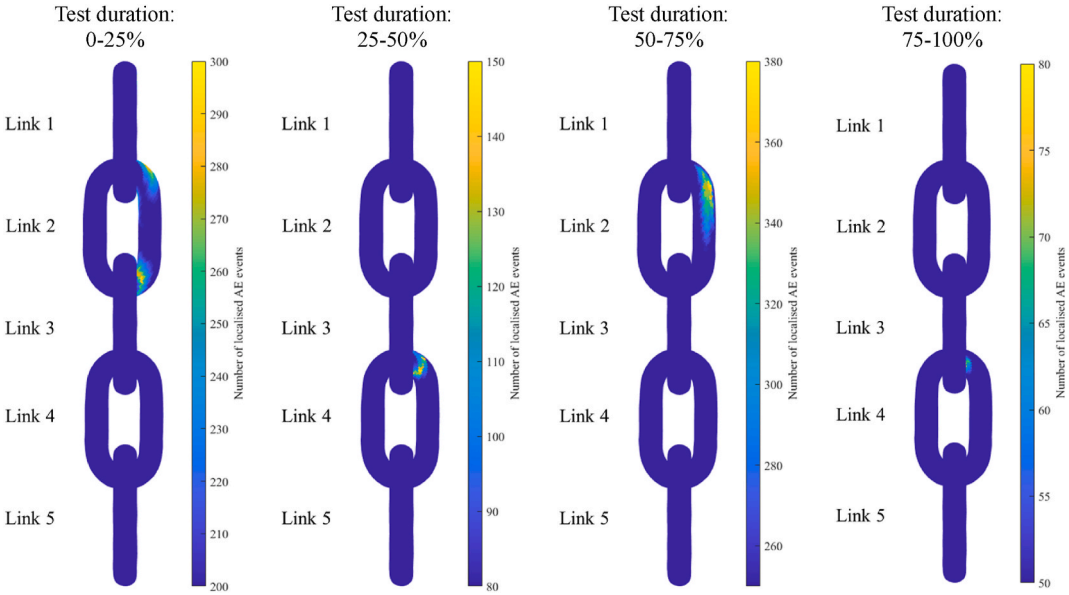

Fig. 8. Localisation map of AE sources for different periods of the test duration.

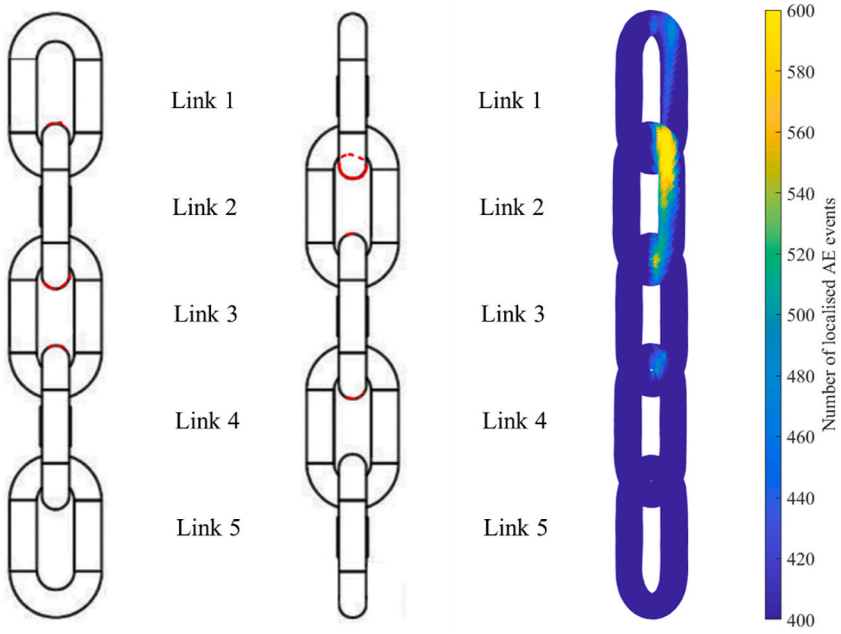

Fig. 9. Total localisation map of AE sources and a sketch showing the main fracture and the observed indications (red circle and red lines respectively) during the post-failure inspection.

When combined with the insights in Fig. 9, it can be inferred that the main AE source localised in Link 1–2 correlates with the main fracture (and linear indications) in the chain segment. The entity of the secondary AE sources (i.e. the number of localised AE events) localised in Link 2–3 and Link 3–4 correlate with the indications observed in the respective areas. All the locations where indications were found through MP testing have been detected and localised using the remote AE technique. Furthermore, there are no indications by the AE that have not been found using MP testing. It can be concluded that a good correlation between the post-failure observation and the AE localisation has been found.

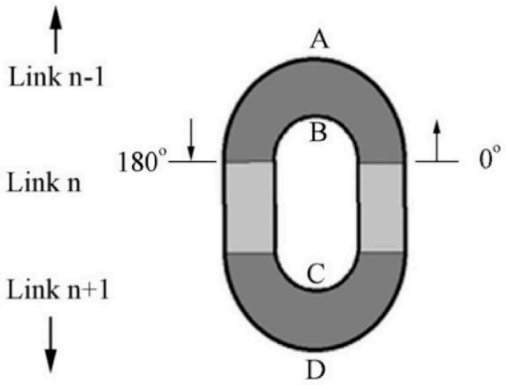

Fig. 10. Positions in each link. Dark grey areas in the sketch were tested.

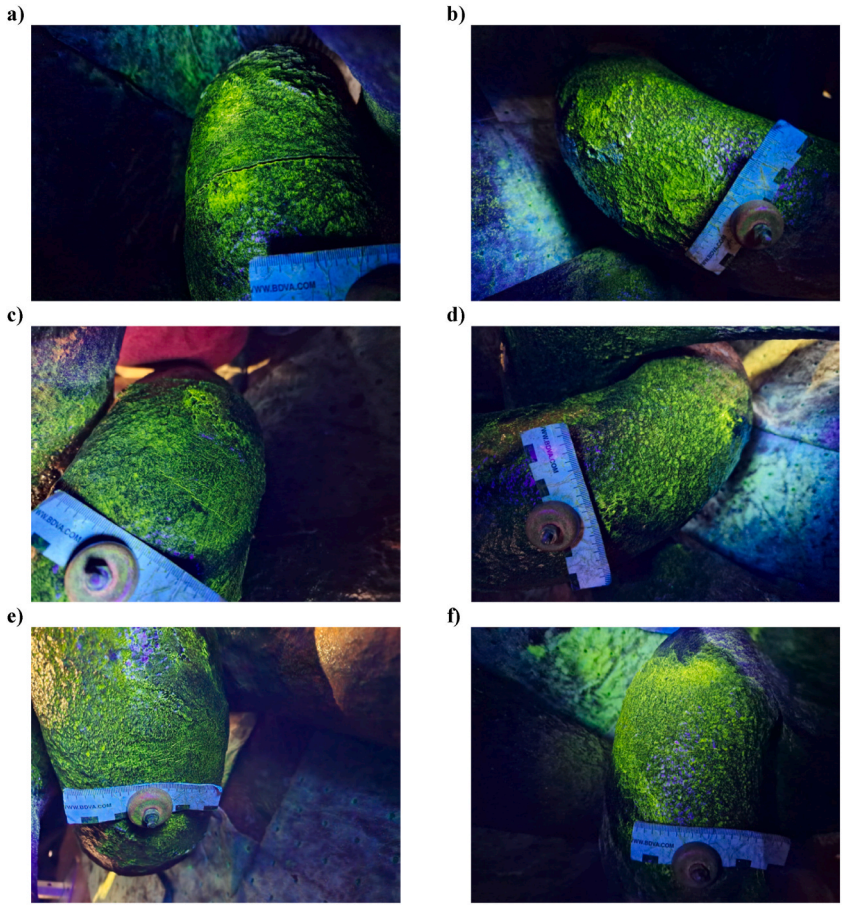

Fig. 11. Results post-failure inspection. (a) Link 1, position D. (b) Link 2, position A. (c) Link 2, position D. (d) Link 3, position A. (e) Link 3, position D. (f) Link 4, position A.

4.4. Envisioned implementation

The proposed approach can provide a qualitative assessment of corrosion-fatigue damage. Future work will be needed for in-situ application of the presented approach to real-world offshore mooring chains. The envisioned application may involve permanent instrumentation of the chain or installing the measurement equipment on remotely-operated underwater vehicles (ROVs). Underwater noise may be more pronounced in offshore conditions due to currents, ship propellers, waves, external operations, etc. Nonetheless, these sources are generally characterised by AE signatures with frequencies predominantly below 100 kHz [53–55], whereas

Table 3
Results of post-failure inspection.

Link	Region	Observations	Shown in Figure
Link 1	D	Fracture and linear indication measuring 12 mm.	Fig. 11a
Link 2	A	Linear indications measuring 6 mm, 4 mm, and several linear indications <2 mm.	Fig. 11b
	D	Linear indications measuring 40 mm, 15 mm, 10 mm, and multiple linear indications <5 mm.	Fig. 11c
Link 3	A	Linear indication measuring 10 mm.	Fig. 11d
	D	Linear indication measuring 10 mm, and multiple linear indications <3 mm.	Fig. 11e
Link 4	A	Linear indications measuring 6 mm, 5 mm, and multiple linear indications <3 mm.	Fig. 11f

corrosion-fatigue-induced AE signals are mostly pronounced in the range of 100–400 kHz. Further investigation will be needed to determine minimum requirements for offshore measurements and acquisition settings.

5. Conclusions

Large-scale corrosion-fatigue experiments were performed to assess the feasibility of detection, localisation, and monitoring of corrosion-fatigue damage in mooring chain links using underwater remote Acoustic Emission (AE) technique. A 5-link mooring chain segment was subjected to cyclic loading while submerged in artificial seawater. Ultrasound signals were continuously measured using a combination of a vertical array of 4× AE transducers and two movable arrays of 4× AE transducers each placed on perpendicular planes.

Parametrisation of the AE measurements was used to monitor the acoustic activity induced by the initiation and growth of corrosion-fatigue damage. The total number of AE signals highlighted the most active area in the test rig, i.e. upper links, attributed to a combination of damage-induced ultrasound signals and noise from the upper clamp. The cumulative number of AE signals displayed distinct activity patterns in the upper and mid-lower sections of the chain segment, with damage-induced ultrasound signals (in the upper part of the chain sample) characterised by two different slopes of the curve (possibly indicating a slow and fast rate of damage growth), and a characteristic AE quiescence in the later stage of the test. The AE hit rate confirmed distinct acoustic activity in the upper and mid-lower sections of the chain segment, with the former showing two levels of AE hit rate during the first (from 0 % to 35 %) and the second part (from 35 % to 85 %) of the test duration.

A 3D source localisation algorithm for damage-induced ultrasound signals was successfully implemented. Results of the AE source localisation were projected on the 3D geometry of the chain segment in the form of a localisation map. The AE source localisation map revealed three distinct zones of acoustic activity. The range of localised AE events varied between 450 and 600 events for the lowest and highest acoustic activity regions, respectively.

A good correlation between the post-failure MP testing and the AE localisation has been found. All the locations where indications were found through MP testing have been detected and localised using the remote AE technique.

While the study demonstrates that growing damage can be effectively detected, localised, and monitored using underwater non-contact AE transducers, improvements in future work will include increasing the number of sensors in the movable arrays and investigating potential masking effects on damage-induced ultrasound signals. Normalisation of the AE source localisation results will be implemented for enhanced comparison of damage monitoring results. Further studies will also be performed to assess the possible relation between the crack size and the AE features (e.g. signal energy, frequency content, etc.). The findings presented in this investigation can serve as the basis for future possible damage prognosis in mooring chain links using underwater remote AE technique.

CRediT authorship contribution statement

Filippo Riccioli: Writing – review & editing, Writing – original draft, Visualization, Validation, Software, Methodology, Investigation, Formal analysis, Data curation, Conceptualization. **Øystein Gabrielsen:** Writing – review & editing, Resources. **Ingrid Skutle Høgsæt:** Writing – review & editing, Resources. **Pedro Silva Barros:** Writing – review & editing, Resources. **Lotfollah Pahlavan:** Writing – review & editing, Supervision, Resources, Project administration, Methodology, Funding acquisition, Conceptualization.

Declaration of competing interest

The authors declare that they have no known competing financial interests or personal relationships that could have appeared to influence the work reported in this paper.

Data availability

Data will be made available on request.

Acknowledgements

This research has been conducted within the framework of DONUT Joint Industry Project (JIP). The project partners are acknowledged for their support and contribution. The authors are grateful to Stian Sigbjørnsen, Øyvind Johannessen, and Tor Jo Landheim for their support and contribution during the preparation and execution of the experiments.

References

[1] Adedipe O, Brennan F, Kolios A. Review of corrosion fatigue in offshore structures: present status and challenges in the offshore wind sector. Renew Sustain Energy Rev 2016;61:141–54. https://doi.org/10.1016/j.rser.2016.02.017.
[2] Fontaine E, Rosen J, Potts A, Ma KT, Melchers R. Scorch jip-feedback on MIC and pitting corrosion from field recovered mooring chain links. In: Offshore technology conference. OnePetro.; 2014. https://doi.org/10.4043/25234-MS.
[3] Ma KT, Shu H, Smedley P, L'Hostis D, Duggal A. A historical review on integrity issues of permanent mooring systems. In: Offshore technology conference. OnePetro; 2013. https://doi.org/10.4043/24025-MS.
[4] Melchers RE, Jeffrey R, Fontaine E. Corrosion and the structural safety of FPSO mooring systems in Tropical waters. In: Proceedings of the australasian structural engineering conference; 2012.
[5] Fontaine E, Kilner A, Carra C, Washington D, Ma KT, Phadke A, Laskowski D, Kusinski G. Industry survey of past failures, pre-emptive replacements and reported degradations for mooring systems of floating production units. In: Offshore technology conference. OnePetro.; 2014. https://doi.org/10.4043/25273-MS.
[6] Du J, Wang H, Wang S, Song X, Wang J, Chang A. Fatigue damage assessment of mooring lines under the effect of wave climate change and marine corrosion. Ocean Eng 2020;206:107303. https://doi.org/10.1016/j.oceaneng.2020.107303.
[7] Assaker JP. Underwater inspection of fixed offshore steel structures. Available online: https://iumi.com/news/iumieye-newsletter-september-2020/underwater-inspection-of-fixed-offshore-steel-structures; 2020.
[8] Rizzo P. NDE/SHM of underwater structures: a review. Adv Sci Technol 2013;83:208–16.
[9] Caines S, Khan F, Shirokoff J. Analysis of pitting corrosion on steel under insulation in marine environments. J Loss Prev Process Ind 2013;26(6):1466–83. https://doi.org/10.1016/j.jlp.2013.09.010.
[10] Forsyth DS. Non-destructive testing for corrosion. Corrosion fatigue and environmentally assisted cracking in aging military vehicles (RTO-AG-AVT-140). 2011.
[11] Bhandari J, Khan F, Abbassi R, Garaniya V, Ojeda R. Modelling of pitting corrosion in marine and offshore steel structures–A technical review. J Loss Prev Process Ind 2015;37:39–62. https://doi.org/10.1016/j.jlp.2015.06.008.
[12] Zawawi NA, Liew MS, Alaloul WS, Shawn LE, Imran M, Toloue I. Non-Destructive testing techniques for offshore underwater decommissioning projects through cutting detection: a state of review. In: SPE symposium: decommissioning and abandonment. OnePetro; 2019. https://doi.org/10.2118/199191-MS.
[13] Calabrese L, Proverbio E. A review on the applications of acoustic emission technique in the study of stress corrosion cracking. Corrosion and Materials Degradation 2020;2(1):1–30. https://doi.org/10.3390/cmd2010001.
[14] Scheeren B, Kaminski ML, Pahlavan L. Evaluation of ultrasonic stress wave transmission in cylindrical roller bearings for acoustic emission condition monitoring. Sensors 2022;22(4):1500. https://doi.org/10.3390/s22041500.
[15] Huijer A, Kassapoglou C, Pahlavan L. Acoustic emission monitoring of carbon fibre reinforced composites with embedded sensors for in-situ damage identification. Sensors 2021;21(20):6926. https://doi.org/10.3390/s21206926.
[16] Van Steen C, Pahlavan L, Wevers M, Verstrynge E. Localisation and characterisation of corrosion damage in reinforced concrete by means of acoustic emission and X-ray computed tomography. Construct Build Mater 2019;197:21–9. https://doi.org/10.1016/j.conbuildmat.2018.11.159.
[17] Scheeren B, Kaminski ML, Pahlavan L. Acoustic emission monitoring of naturally developed damage in large-scale low-speed roller bearings. Struct Health Monit 2023;23(1):360–82. https://doi.org/10.1177/14759217231164912.
[18] Pahlavan PL, Paulissen J, Pijpers R, Hakkesteegt H, Jansen R. Acoustic emission health monitoring of steel bridges. In: EWSHM-7th European workshop on structural health monitoring; 2014.
[19] Grosse C. Acoustic emission testing. https://doi.org/10.1007/978-3-540-69972-9; 2008.
[20] Yuyama S, Hisamatsu Y, Kishi T. Fundamental aspects of AE monitoring on corrosion fatigue processes in austenitic stainless steel. J Mater Energy Syst 1984;5(4). https://doi.org/10.1007/BF02835719.
[21] Chai M, Hou X, Zhang Z, Duan Q. Identification and prediction of fatigue crack growth under different stress ratios using acoustic emission data. Int J Fatig 2022;160:106860. https://doi.org/10.1016/j.ijfatigue.2022.106860.
[22] Chai M, Zhang J, Zhang Z, Duan Q, Cheng G. Acoustic emission studies for characterization of fatigue crack growth in 316LN stainless steel and welds. Applied acoustics 2017;126:101–13. https://doi.org/10.1016/j.apacoust.2017.05.014.
[23] Chang H. Acoustic emission study of corrosion fatigue crack propagation mechanism identification. Appl Mech Mater 2014;628:20–3. https://dx.doi.org/10.4028/www.scientific.net/AMM.628.20.
[24] Chang H, Han E, Wang JQ, Ke W. Acoustic emission study of corrosion fatigue crack propagation mechanism for LY12CZ and 7075-T6 aluminum alloys. J Mater Sci 2005;40:5669–74. https://doi.org/10.1007/s10853-005-1300-9.
[25] Hwang W, Bae S, Kim J, Kang S, Kwag N, Lee B. Acoustic emission characteristics of stress corrosion cracks in a type 304 stainless steel tube. Nucl Eng Technol 2015;47(4):454–60. https://doi.org/10.1016/j.net.2015.04.001.
[26] Chai M, Lai C, Xu W, Duan Q, Zhang Z, Song Y. Characterization of fatigue crack growth based on acoustic emission multi-parameter analysis. Materials 2022;15(19):6665. https://doi.org/10.3390/ma15196665.
[27] Calabrese L, Bonaccorsi L, Galeano M, Proverbio E, Di Pietro D, Cappuccini F. Identification of damage evolution during SCC on 17-4 PH stainless steel by combining electrochemical noise and acoustic emission techniques. Corrosion Sci 2015;98:573–84. https://doi.org/10.1016/j.corsci.2015.05.063.
[28] Bi H, Li H, Zhang W, Wang L, Zhang Q, Cao S, Toku-Gyamerah I. Evaluation of the acoustic emission monitoring method for stress corrosion cracking on aboveground storage tank floor steel. Int J Pres Ves Pip 2020;179:104035. https://doi.org/10.1016/j.ijpvp.2019.104035.
[29] Aggelis DG, Kordatos EZ, Matikas TE. Acoustic emission for fatigue damage characterization in metal plates. Mech Res Commun 2011;38(2):106–10. https://doi.org/10.1016/j.mechrescom.2011.01.011.
[30] Du G, Li J, Wang WK, Jiang C, Song SZ. Detection and characterization of stress-corrosion cracking on 304 stainless steel by electrochemical noise and acoustic emission techniques. Corrosion Sci 2011;53(9):2918–26. https://doi.org/10.1016/j.corsci.2011.05.030.
[31] Chang H. Identification of damage mode in AZ31 magnesium alloy under tension using acoustic emission. Trans Nonferrous Metals Soc China 2015;25(6):1840–6. https://doi.org/10.1016/S1003-6326(15)63790-6.
[32] Skal's' Kyi VR, Nazarchuk ZT, Dolins' ka IY, Yarema RY, Selivonchyk TV. Acoustic-emission diagnostics of corrosion defects in materials (a survey). Part. 1. Detection of electrochemical corrosion and corrosion fatigue. Mater Sci 2017;53:295–305. https://doi.org/10.1007/s11003-017-0075-x.
[33] Han Z, Luo H, Cao J, Wang H. Acoustic emission during fatigue crack propagation in a micro-alloyed steel and welds. Materials Science and Engineering: A. 2011;528(25–26):7751–6. https://doi.org/10.1016/j.msea.2011.06.065.
[34] Li L, Zhang Z, Shen G. Influence of grain size on fatigue crack propagation and acoustic emission features in commercial-purity zirconium. Materials Science and Engineering: A. 2015;636:35–42. https://doi.org/10.1016/j.msea.2015.03.046.
[35] Fregonese M, Idrissi H, Mazille H, Renaud L, Cetre Y. Initiation and propagation steps in pitting corrosion of austenitic stainless steels: monitoring by acoustic emission. Corrosion Sci 2001;43(4):627–41. https://doi.org/10.1016/S0010-938X(00)00099-8.
[36] Jirarungsatian C, Prateepasen A. Pitting and uniform corrosion source recognition using acoustic emission parameters. Corrosion Sci 2010;52(1):187–97. https://doi.org/10.1016/j.corsci.2009.09.001.

[37] Rivera FG, Edwards G, Eren E, Soua S. Acoustic emission technique to monitor crack growth in a mooring chain. Appl Acoust 2018;139:156–64. https://doi.org/10.1016/j.apacoust.2018.04.034.
[38] Angulo Á, Tang J, Khadimallah A, Soua S, Mares C, Gan TH. Acoustic emission monitoring of fatigue crack growth in mooring chains. Appl Sci 2019;9(11):2187. https://doi.org/10.3390/app9112187.
[39] Sutowski P, Nadolny K, Kaplonek W. Monitoring of cylindrical grinding processes by use of a non-contact AE system. Int J Precis Eng Manuf 2012;13:1737–43. https://doi.org/10.1007/s12541-012-0228-7.
[40] Schmidt PL, Nelson JK, Handy RG, Morrell JS, Jackson MJ, Rees TM. Noncontact measurements of acoustic emissions from the single-point turning process. Int J Adv Des Manuf Technol 2017;93:3907–20. https://doi.org/10.1007/s00170-017-0756-5.
[41] Matsuo T, Hatanaka D. Development of non-contact fatigue crack propagation monitoring method using air-coupled acoustic emission system. Eng Trans 2019; 67(2):185–98. https://doi.org/10.24423/EngTrans.1009.20190405.
[42] Xiao W, Yu L. Non-contact passive sensing of acoustic emission signal using the air-coupled transducer. Health Monitoring of Structural and Biological Systems XV 2021;11593:12–419. https://doi.org/10.1117/12.2583218.
[43] Alkhateeb S, Riccioli F, Morales FL, Pahlavan L. Non-contact acoustic emission monitoring of corrosion under marine growth. Sensors 2022;23(1):161. https://doi.org/10.3390/s23010161.
[44] Riccioli F, Pahlavan L. Non-contact acoustic emission monitoring of corrosion-fatigue damage in submerged steel structures. Struct Health Monit 2023. https://doi.org/10.12783/shm2023/36856.
[45] Terchi A, Au YHJ. Acoustic emission signal processing. Measurement and Control, vol. 34; 2001. p. 240–4. 8.
[46] Ohtsu M, Enoki M, Mizutani Y, Shigeishi M. Principles of the acoustic emission (AE) method and signal processing. In: Practical acoustic emission testing. Tokyo: Springer Japan; 2016. p. 5–34. https://doi.org/10.1007/978-4-431-55072-3_2.
[47] Kundu T. Acoustic source localization. Ultrasonics 2014;54(1):25–38. https://doi.org/10.1016/j.ultras.2013.06.009.
[48] Akaike H. Markovian representation of stochastic processes and its application to the analysis of autoregressive moving average processes. Ann Inst Stat Math 1974;26:363–87. https://doi.org/10.1007/BF02479833.
[49] Kurz JH, Grosse CU, Reinhardt HW. Strategies for reliable automatic onset time picking of acoustic emissions and of ultrasound signals in concrete. Ultrasonics 2005;43(7):538–46. https://doi.org/10.1016/j.ultras.2004.12.005.
[50] ASTM E976-15. Standard guide for determining the reproducibility of acoustic emission sensor response. West Conshohocken, PA, USA: American Society of Testing of Materials; 2015.
[51] Pullin R, Eaton MJ, Hensman JJ, Holford KM, Worden K, Evans SL. Validation of acoustic emission (AE) crack detection in aerospace grade steel using digital image correlation. Appl Mech Mater 2010;24:221–6.
[52] Gagar DO. Validation and verification of the acoustic emission technique for structural health monitoring. http://dspace.lib.cranfield.ac.uk/handle/1826/8402; 2013.
[53] Cruz E, Lloyd T, Bosschers J, Lafeber FH, Vinagre P, Vaz G. Study on inventory of existing policy, research and impacts of continuous underwater noise in Europe. WavEC Offshore Renewables and Maritime Research Institute Netherlands; 2021. EMSA report EMSA/NEG/21/2020.
[54] Huang LF, Xu XM, Yang LL, Huang SQ, Zhang XH, Zhou YL. Underwater noise characteristics of offshore exploratory drilling and its impact on marine mammals. Front Mar Sci 2023;10:1097701.
[55] Jiménez-Arranz G, Banda N, Cook S, Wyatt R. Review of existing data on underwater sounds produced by the oil and gas Industry. JIP topic-sound source characterisation and propagation; 2020.